

Enhanced ionization in small rare-gas clusters

Christian Siedschlag and Jan M. Rost

Max-Planck-Institute for the Physics of Complex Systems, Nöthnitzer Strasse 38, D-01187 Dresden, Germany

(Received 2 July 2002; revised manuscript received 12 September 2002; published 17 January 2003)

A detailed theoretical investigation of rare-gas atom clusters under intense short laser pulses reveals that the mechanism of energy absorption is akin to *enhanced ionization* first discovered for diatomic molecules. The phenomenon is robust under changes of the atomic element (neon, argon, krypton, xenon), the number of atoms in the cluster (16–30 atoms have been studied), and the fluence of the laser pulse. In contrast to molecules it does not disappear for circular polarization. We develop an analytical model relating the pulse length for maximum ionization to characteristic parameters of the cluster.

DOI: 10.1103/PhysRevA.67.013404

PACS number(s): 42.50.Hz, 36.40.–c, 33.80.–b

I. INTRODUCTION

Building the bridge between atomic and solid-state physics, cluster physics has become a vivid research field of its own. While the static properties of clusters are by now well understood, there remain open problems concerning the dynamics of clusters under external perturbations. Linear-response theory has proven to be a valid tool for the investigation of dynamical properties under weak perturbations [1]. However, with increasing strength of the perturbation, the description of the cluster evolution becomes more and more involved [2].

On the other hand, experimental studies of (mostly) rare-gas clusters interacting with highly charged projectiles [3] as well as with short, intense laser pulses have produced a number of interesting results calling for an explanation. Rare-gas clusters exposed to intense laser light have shown a big increase of energy absorption compared to the single-atom case [4–9]. When irradiated with a 10^{15} -W/cm² femtosecond laser pulse whose wavelength is in the optical regime, one observes, depending on the cluster size and the atomic element, ionic charge states of up to 40. These high charge states let the fragmenting ions gain an enormous amount of kinetic energy. The most spectacular example of this highly energetic process has certainly been the recent experimental observation of nuclear fusion in a cluster [10].

Here, we focus on clusters of some 10 atoms. We have developed a model containing the essential features of the interaction between the cluster and the laser field. The main findings have been reported briefly in Ref. [11]; namely, that energy absorption from the laser pulse proceeds through a mechanism originally discovered for diatomic molecules (*enhanced ionization* (ENIO) [12,13]). However, there are differences, e.g., ENIO has on clusters a similar effect for both linear and circular polarization of the laser.

An enhancement of ionization has also been observed for a model of a linear chain of up to seven atoms by Veniard *et al.* [14]. Most likely this enhancement is due to the same ENIO mechanism that we will discuss here, while the enhancement reported in Refs. [15,16] for a cluster of several hundred atoms has been attributed to a different mechanism of collective electron motion.

We will give a detailed account of our approach and discuss results for a number of different elements as well as for

different parameters of the laser pulse. Qualitatively similar to the full dynamical simulation of Ref. [16], but in contrast to Ref. [15], we describe the entire process including initial ionization fully dynamically. That is, we neither fix *a priori* and by hand the nuclei nor the number of ionized electrons. However, we will also address the case of fixed nuclei since it is the traditional way to detect ENIO [12,13]. Our investigations allow us to formulate a relatively simple analytical model that relates the maximum electron release in rare-gas atom clusters to an optimal pulse length.

The paper is organized as follows: after introducing the numerical model and comparing it to other approaches in Sec. II, we investigate the dependence of energy absorption and ionization yield on the pulse length in a series of clusters in Sec. III. From the results of these calculations a generic behavior emerges, which can be explained by invoking the above-mentioned enhanced ionization mechanism as explained in Sec. IV. We give strong evidence that this mechanism should play an important role in the laser-cluster interaction over a wide range of parameters detailed in Sec. V. Finally we condense our picture of the ionization process into a simple analytical expression that quantifies the role of the experimentally accessible variables such as the cluster size or atomic element in the process of energy absorption in Sec. VI. Section VII summarizes our work. Atomic units are used if not stated otherwise.

II. THE CLUSTER MODEL**A. Theoretical formulation and numerical implementation**

Since the dimension of the problem is far too high to allow for an exact quantum-mechanical treatment, we have formulated a model to describe the dynamics of rare-gas clusters in strong laser fields. We resort to a classical treatment, with a few but essential quantum-mechanical elements.

Initially, before the onset of the laser pulse, we compute the equilibrium ground-state configuration of the cluster with Lennard-Jones interactions between the neutral cluster atoms. One can find the global potential minimum for a certain cluster by propagating the atoms while cooling down the system so it relaxes to the global minimum. However, the global minima for this type of interaction are also readily

available in the literature [30]. The electrons are assumed to be localized at the nuclei.

After fixing the initial shape of the cluster, we start the time evolution switching on the laser pulse (from this moment on, the contribution of the Lennard-Jones potential is neglected). For the electrons, the evolution consists of two parts: first, the modeling of the bound state and the process of ionization from this state; second, the propagation after being ionized from an atom. We will refer to the first process as *inner ionization*, in contrast to the *outer ionization*, which has the effect that an electron leaves the cluster [15]. Inner ionization encompasses processes beyond classical mechanics, while the subsequent propagation and (eventually) outer ionization is described classically via the integration of Newton's equations.

When irradiating a cluster with intense laser light, two processes can lead, at least in principle, to inner ionization: *field ionization* and *electron-impact ionization*. In the case of field ionization, the electric field inside the cluster (initially only the laser field, later the combined field of laser, ions and electrons) leads to a lowering of the potential barriers, so that an electron can leave its mother atom via tunneling [17] or even *over-the-barrier* [18]. Electrons that are already inner ionized, but not yet outer ionized, can further lead to electron-impact ionization. This mechanism was shown to play almost no role in small clusters [19], as the average free path length with respect to electron-impact ionization is much larger than the cluster radius. For this reason we consider field ionization only.

The model is implemented as follows. Before the onset of the pulse the electrons of the cluster are assumed to be localized at the atomic positions; the bare nucleus and all the electrons of an atom are treated as one neutral classical particle. It is only later that the electrons (through inner ionization) are born as separate classical particles. Hence, the number of particles in our simulation changes with time.

A classical charged particle j at position \vec{r}_j interacts with another charged particle i at \vec{r}_i via the potential

$$V_i^j \equiv V(\vec{r}_j, \vec{r}_i) = \frac{Z_i Z_j}{(|\vec{r}_i - \vec{r}_j|^2 + a_{Z_i} + a_{Z_j})^{1/2}}, \quad (1)$$

where Z_i and Z_j are the charges of the two particles. The a_{Z_i} are Z -dependent soft-core parameters, which help to regularize the Coulomb singularity. For an electron with charge $Z_e = -1$, we define $a_{-1} = 0.1$. If the potential Eq. (1) describes the outermost electron bound to an atom ($Z = +1$) or ion of charge Z , we determine a_Z from the energy balance

$$-Z(a_Z + a_{-1})^{-1/2} = E_{\text{bind}}(Z) + \epsilon, \quad (2)$$

where $\epsilon = 0.01$ is a small positive parameter.

At every time step dt , we calculate for each atom $j = 1, \dots, N$, the ionization probability of the outermost electron from tunneling through the instant potential landscape U_j in the direction $\hat{e}_{B_j} = \vec{B}_j / |\vec{B}_j|$ of the instant electric field \vec{B}_j , which would be felt by the bound electron at the position

\vec{r}_j of atom j . The instant electric field contains contributions from all charged particles and the laser field,

$$\vec{B}_j = \vec{\nabla}_{\vec{r}_j} \sum_{i \neq j} V_i^j + \vec{\epsilon}_p f(t), \quad (3)$$

where $\vec{\epsilon}_p$ is the laser polarization vector and $f(t)$ is the electric field of the laser pulse whose exact form we will discuss later. The tunneling integral reads now

$$I_j(t) = \exp \left[-2 \int_{r_-}^{r_+} \sqrt{2(U_j(r) - E_n^j)} dr \right], \quad (4)$$

where r_{\pm} are the inner ($-$) and outer ($+$) turning points defined by $U_j(r_{\pm}) = 0$. The potential landscape U_j is given by

$$U_j(r) = \sum_{i \neq j} V_i^j(\vec{r}_j + r \hat{e}_{B_j}, \vec{r}_i) + (\vec{r}_j + r \hat{e}_{B_j}) \cdot \vec{\epsilon}_p f(t). \quad (5)$$

The energy level E_n^j is not the pure atomic level $E_n^{Z_j}$, rather it is shifted by the surrounding charge and the laser potential while the potential of the atom from which the electron will be ionized has to be subtracted because its influence is already contained in E_n^Z :

$$E_n^j := E_n^{Z_j} + U_j(0) - \frac{Z_j + 1}{\sqrt{a_{Z_j} + 0.1}}. \quad (6)$$

The classical turning points r_{\pm} are determined numerically and the search for r_+ is continued until $I(t) < 10^{-10}$. If we find a position r' with $dU_j/dr|_{r=r'} = 0$ and $E_n^j > U_j(r)$ for $r \leq r'$, over-the-barrier ionization is possible. In this case the "tunneling" probability is $I(t) = 1$.

The tunneling rate $w(t)$ is the tunneling probability $I(t)$ multiplied by the frequency of the electron hitting the potential barrier. In a semiclassical picture, this frequency is the inverse of the Kepler period T_n belonging to an orbit with binding energy E_n ,

$$T_n = \pi(Z+1)/(2E_n^3)^{1/2}. \quad (7)$$

Hence, the tunneling rate is $w(t) = I(t)/T_n$. The tunneling probability over a unit of time dt is $P(t) = w(t)dt$. By comparison with a random number z [Is $P(t) > z$?] we decide if the electron in question tunnels. If so, we place the electron, which now becomes a classical particle, outside the potential barrier as close to r_+ as possible, with the exact position and momentum of the electron determined by conservation of the total energy. If the ionization happens to be over the barrier, we put the electron on top of the barrier, where $dU_j/dr = 0$. The atomic charge is raised by 1 and the next virtual electron is allowed to tunnel.

The particles are classically propagated by integrating Newton's equations of motion. We have used a symplectic integrator [20] with a time step of $dt = 0.1$.

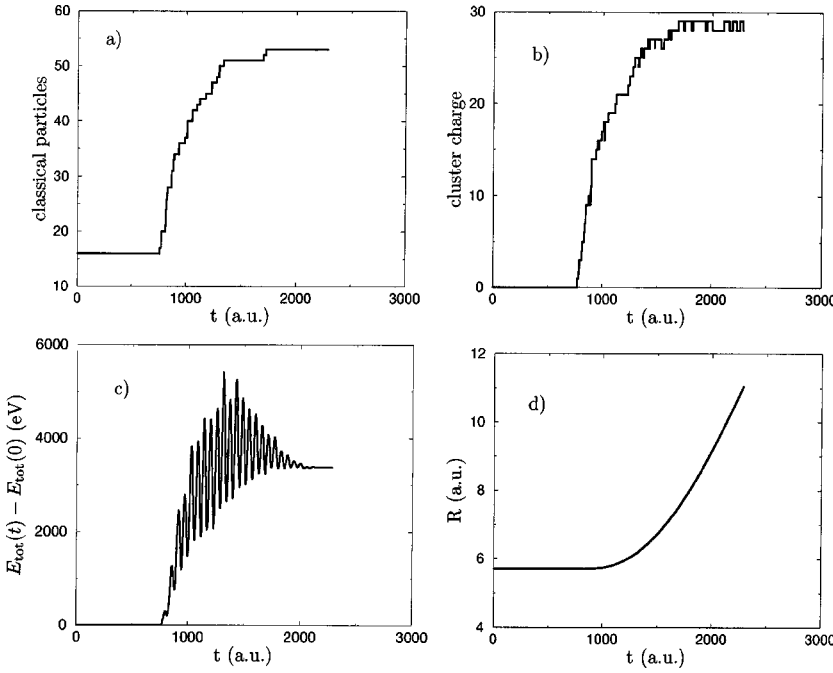


FIG. 1. Time evolution of the number of classically treated particles (a), total charge of the cluster (b), absorbed energy (c) in terms of the cluster energy [Eq. (9)], and cluster radius (d) in terms of average interionic distance [Eq. (11)] during a single run.

B. A typical run

Although later we will calculate experimentally accessible observables with a Monte Carlo ensemble, for a qualitative understanding of the phenomena it is sufficient to have a closer look on a single event, since the overall behavior of the ensemble members is quite similar. As an example we consider a Ne_{16} cluster. The applied pulse has a peak intensity of $I=10^{15}$ W/cm², a frequency of $\omega=0.055$ a.u. (780 nm), and it extends over 20 cycles, so that the pulse length $T\approx 55$ fs. We chose a \sin^2 function for the pulse envelope, i.e., the pulse is of the form

$$f(t) = F \sin^2(\pi t/T) \sin(\omega t) \quad (0 \leq t \leq T). \quad (8)$$

Figure 1 shows typical observables obtained from a single run during the laser pulse. After ≈ 750 a.u. the intensity of the laser is sufficiently high for the first inner ionization event, followed by a rapid increase in the number of classical particles [Fig. 1(a)] as well as the cluster charge [Fig. 1(b)]. Obviously, the ionization of the first few electrons leads to an “avalanche effect”: the inner ionized electrons produce ions and together they create a strong electric field inside the cluster, which helps to inner ionize further electrons (this is reminiscent of the *ionization ignition* mechanism [21]). The absorbed energy is the difference of the cluster energy E_{tot} before and after the laser pulse [Fig. 1(c)]. As we can see, this rather small cluster can already absorb a considerable amount of energy. The oscillations are due to the laser amplitude $f(t)$ and have no direct influence on the net energy absorption. If \mathcal{K} is the set of nuclei with mass M , \mathcal{E} is the set of inner ionized electrons already treated classically, and \mathcal{G} is the set of electrons that are still bound, the cluster energy E_{tot} is defined as

$$E_{\text{tot}} = \sum_{i \in \mathcal{K}} \frac{P_i^2}{2M} + \sum_{i \in \mathcal{E}} \frac{p_i^2}{2} + \sum_{i,j \in \mathcal{K} \cup \mathcal{E}} V_{ij} + \sum_{i \in \mathcal{G}, n} E_n^i \quad (9)$$

$$+ \sum_{i \in \mathcal{K}} Z_i (\vec{\epsilon}_p \cdot \vec{r}_i) f(t) - \sum_{i \in \mathcal{E}} (\vec{\epsilon}_p \cdot \vec{r}_i) f(t) \quad (10)$$

with the E_n^i from Eq. (6). As the cluster gets charged, it begins to expand, i.e., the mean interionic distance, defined as

$$R(t) = \left(\frac{1}{N} \sum_{i=1}^N \min_{i \neq j} \{ |\vec{r}_i - \vec{r}_j|^2 \} \right)^{1/2} \quad (11)$$

for a cluster of N atoms, will increase [Fig. 1(d)].

At the intensity used here, the cluster disintegrates completely, i.e., we observe only atomic fragments after the pulse. Note that the expansion of the cluster takes place adiabatically compared to the time scales of the laser frequency and the electronic motion, but on the same time scale as the pulse length. Hence, it is possible to explore radius-dependent properties of the cluster by varying the pulse length.

C. Comparison to other models

Almost all existing models for small rare-gas clusters in strong laser fields rely essentially on classical mechanics. The main differences lie in the treatment of inner ionization. Rose-Petruck *et al.* [21] used a fully classical description without tunneling. Instead, inner ionization occurs by the deformation of the Kepler orbit of the active bound electron through the laser field and the surrounding charges. Neglecting any tunneling contributions, the first inner ionization will take place a certain time Δt later than in our case. As we will see, this delay can have a significant influence on the subsequent dynamics of the cluster rendering a fully classical treatment problematic.

In a later approach Ditmire [22] approximated the tunneling contribution by the Landau rate for a bound electron in

an external field [23]. In this case, inner ionization occurs if the local field strength at the position of the atom is strong enough. Hence, an electron that comes by chance close to an ion will create *locally* such a strong field that ionization can hardly be avoided while in our formulation the entire environment of an atom, i.e., the mean field must be suitable for ionization. Consequently, we get lower ionization rates than in Ref. [22] but in better agreement with Ref. [19] that contains probably the most complete quasiclassical formulation to date. The authors of Ref. [19] treat tunneling as we do, but use the full Coulomb interaction instead of soft-core potentials. This leads to the problem of unphysical classical autoionization due to the missing lower bound in energy provided quantum mechanically by the uncertainty relation. In Ref. [19] this problem is avoided by invoking a mechanism that recaptures the (classical) electrons into virtual bound states. Although our approach and that of Ref. [19] differ in the modeling of the forces and processes governing the electron dynamics, the ionization yields agree surprisingly well.

III. ABSORPTION PROPERTIES FOR DIFFERENT PULSE LENGTHS

To investigate how the expansion of a cluster during the interaction with a strong laser pulse influences its absorption behavior, we have calculated the absorbed energy and the average ionic charges after the interaction for various pulse lengths. To keep the amount of energy delivered by these pulses fixed, we demand the fluence to be constant, i.e.,

$$E(T) = \int_0^T f^2(t) dt = \text{const.} \quad (12)$$

For a pulse of the shape of Eq. (8), one has $E(T) = 3F^2T/16$ from Eq. (12). For the reference pulse, we chose the parameters already used in the single run from the preceding section: $F=0.16$ a.u., $\omega=0.055$ a.u., and a pulse length of 20 cycles. Shorter pulses have a higher maximum field strength and longer pulses have a lower maximum field strength. The results were obtained by averaging over a Monte Carlo ensemble consisting of 20 clusters.

The absorbed energy and the average atomic charges as a function of pulse length under the constraint of Eq. (12) are shown in Figs. 2 and 3, respectively, for clusters of $N=16$ atoms. The light Ne_{16} exhibits a monotonic decrease in energy and charge as functions of the pulse length characteristic for atoms. In contrast the heavier clusters, Ar_{16} , Kr_{16} , and Xe_{16} show typical cluster properties with a maximum at a certain pulse length T^* after an initial decrease in the yield. The maximum average charge per atom reached at T^* is with 4.5 for argon and almost 7 for xenon considerably larger than for the respective isolated atom.

The maximum is much more pronounced for the ionization yield than for the absorbed energy for two reasons. First, for shorter pulses the mean internuclear distance just after the pulse will in general be smaller than for longer pulses, so that the Coulomb explosion energy will increase with decreasing pulse length. Second, the ionized electrons, which can be considered to be quasifree, acquire a higher kinetic

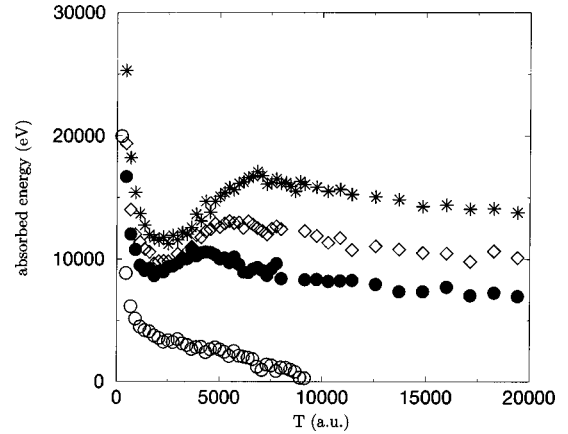


FIG. 2. Energy absorption of Ne_{16} (\circ), Ar_{16} (\bullet), Kr_{16} (\diamond), and Xe_{16} ($*$) for different pulse lengths (see text).

energy for shorter pulses, since the intensity is higher than for longer pulses. These two effects wash out the minimum in the curve for the absorbed energy and decrease the contrast between the minimum and the maximum.

IV. CALCULATIONS WITH FIXED NUCLEI

The existence of an optimal pulse length T^* can be easily understood if an optimal cluster geometry with a critical interionic distance R^* exists, which maximizes the energy absorption (and also the ionization). For short pulse lengths, the cluster hardly expands during the pulse and the critical distance will be reached only well after the end of the pulse (provided R^* is larger than the equilibrium distance R_0). For longer pulses, the cluster will reach R^* during the pulse. For a certain pulse length T^* , the time of reaching R^* will roughly coincide with the maximum of the pulse, which leads to optimal absorption. If the pulses are becoming even longer, R^* will be reached already before the maximum of the pulse. Moreover, the maximum intensity is decreasing due to the energy normalization [Eq. (12)]. Both effects lead to a decrease in energy absorption as well as in the average atomic ionization for $T > T^*$.

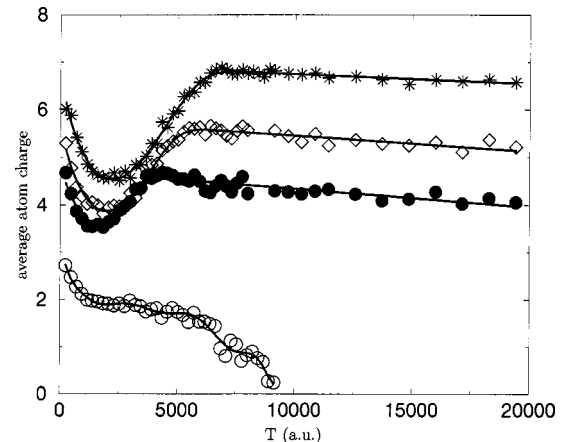


FIG. 3. Average atom charge as a function of pulse lengths for different clusters; see Fig. 2. The solid lines are to guide the eye.

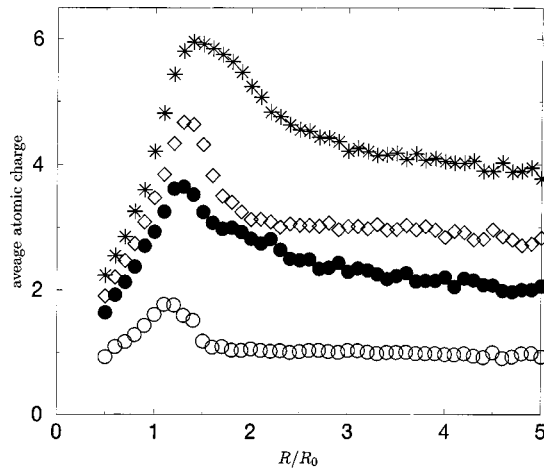


FIG. 4. Average atomic charge, calculated with fixed nuclei, as a function of the mean interionic distance [see Eq. (11), in units of the equilibrium mean interionic distance R_0] for Ne_{16} (\circ), Ar_{16} (\bullet), Kr_{16} (\diamond) and Xe_{16} ($*$).

What remains is to show that a critical distance R^* really exists and to explain its origin. To this end, we have calculated the cluster ionization yield for *different*, but *fixed* interionic distance. We have accomplished this by applying a scaling transformation

$$\vec{r}_i^0 \Rightarrow \lambda \vec{r}_i^0 \quad (13)$$

to the atomic positions, with $\lambda=1$ corresponding to the ground-state configuration. The pulse we use is the reference pulse for the calculations of the last section, i.e., of the form Eq. (8) with $F=0.16$ a.u., $\omega=0.055$ a.u., and 20 cycles length. For all four clusters under consideration, we observe the existence of a critical R^* that is larger than the equilibrium one (Fig. 4). Hence, R^* can be reached during the cluster expansion and the results of the preceding section can indeed be explained by the existence of R^* .

Finally, we ask why R^* exists. Two mechanisms could be operative: first, a resonance effect where the electrons inside the cluster oscillate at a certain characteristic frequency that would coincide with the laser frequency at a certain cluster size. This kind of mechanism is well known from the plasmon resonance in metal clusters [24]; being originally a weak-field-concept, the plasmon has been claimed to play an important role also in the strong-field regime [4]. However, one needs a delocalized electron cloud to create a plasmon resonance; in small rare-gas clusters, this condition is not fulfilled. Similarly, the quasiresonance mechanism of Refs. [15,16] needs a large number of inner ionized electrons that remain in the cluster. This requirement is not fulfilled for the smaller clusters we describe here. The second mechanism would be a generalization of a concept first discovered for diatomic molecules [12,25,13], called ENIO. It can be qualitatively explained by looking at the potential curve of a homonuclear diatomic molecule exposed to a quasistatic electric field (see Fig. 5): the upper energy level of the two levels $1\sigma_+$ and $1\sigma_-$, which emanate from the bonding and the antibonding molecular orbital when an electric field is

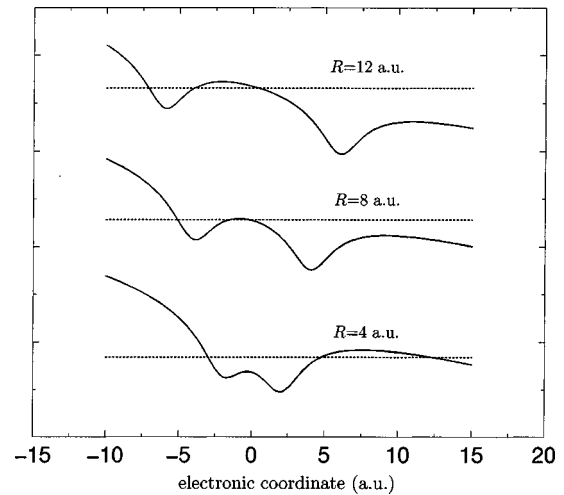


FIG. 5. Schematic potential curves and the upper energy level $1\sigma_-$ of a diatomic molecule for different internuclear distances.

switched on, will lie above the inner potential barrier but below the outer potential barrier when the internuclear distance R is small. On the other hand, when R is large, the level will lie below the inner barrier but above the outer barrier (using the terms introduced in the preceding section, we can say that *inner ionization* is easier than *outer ionization* for small R and vice versa for large R). For an intermediate value of R , typically around 6–8 a.u., the interplay between the inner and outer ionizations will lead to a maximum in the ionization rate.

This mechanism has been shown to be operative not only in linear molecules and a linear chain of atoms [14], but also in triatomic molecules of triangular shape [26,27]. In this case, the simple picture of Fig. 5 is already slightly distorted, and it is more appropriate to think of enhanced ionization in terms of an optimal balance between the inner and outer ionizations, which makes the generalization of the mechanism to a true many-body system such as a cluster much easier.

One characteristic feature of the enhanced ionization mechanism is its relative insensitivity to the frequency of the applied laser field. As long as the quasistatic picture is valid, the value of R^* should not change significantly with the laser frequency. On the other hand, any resonance-type mechanism such as the plasmon picture should exhibit a strong dependence of R^* on the laser frequency. As shown in Fig. 6 the ionization yield of Ar_{16} for three different frequencies peaks at almost the same R^* . Hence, we can exclude any kind of resonance behavior in favor of the enhanced ionization mechanism.

Although the position of R^* does not change with the laser frequency, the absolute ionization yield does. This is due to the fact that electrons which are already outer ionized tend to leave the cluster region faster when the frequency is smaller: the quiver amplitude of an electron in an electric field of frequency ω is proportional to $1/\omega^2$. Hence, on average, in fields of higher frequencies the already ionized electrons will stay closer to the cluster for a longer time and lead to an increased field-ionization rate.

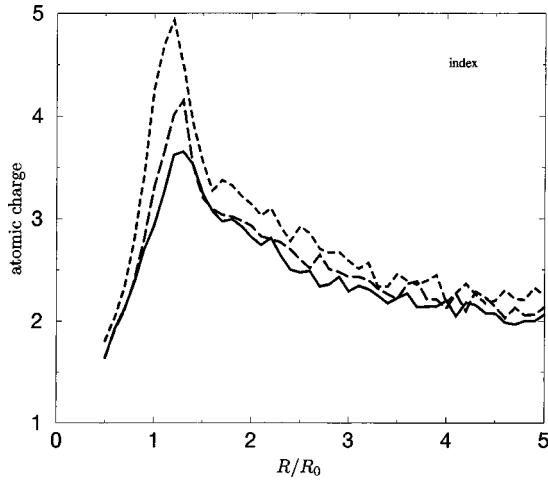


FIG. 6. Atomic ionization yield for the three frequencies $\omega = 0.055$ a.u. (solid line), $\omega = 0.075$ a.u. (long dashed line), and $\omega = 0.11$ a.u. (dashed line) for Ar_{16} . The pulse length was $T = 55$ fs.

V. EXPLORATION OF THE PARAMETERS CONTROLLING LASER-CLUSTER INTERACTION

Having established the basic mechanism for coupling energy from the laser pulse into small rare-gas clusters, we will explore now the influence of different parameters on this mechanism, such as cluster size, energy content of the laser pulse, and laser polarization.

A. Different cluster sizes

First, we present the cluster response with fixed nuclei. The average atomic charge and the absorbed energy were calculated as functions of the mean interionic distance Eq. (11) analogous to Sec. IV. The equilibrium value R_0 does hardly change when going to bigger clusters. The variation of R_0 for Ne_{16} , Ne_{20} , Ne_{25} , and Ne_{30} is only about 0.01 a.u. We have used the same pulse as in Sec. IV. As can be seen from Fig. 7 the bigger clusters show almost no difference compared to Ne_{16} when the energy is normalized to the number of cluster atoms. In particular, the existence of a critical distance $R^* > R_0$ is confirmed in all cases.

There is no hint on a transition to a collective behavior at these cluster sizes. If we think of cluster physics as the transition regime between atomic and solid-state physics, we are still on the atomic side with a cluster of 30 atoms.

From the fact that the charge per atom is almost independent of the number of cluster atoms we may conclude that only the next-neighbor atoms participate in the mechanism of enhanced ionization; otherwise the effectivity of this mechanism should change with the cluster size. The absorbed energy per atom, however, is varying with the number of atoms. This effect can be easily understood by calculating the change in the potential energy $U(N)$ of a cluster consisting of N ions of charge Z and distance R if one adds a new ion with the same charge Z to the cluster. If one assumes that this new ion is placed at the border of the cluster, then

$$U(N+1) = U(N) + NZ^2/R. \quad (14)$$

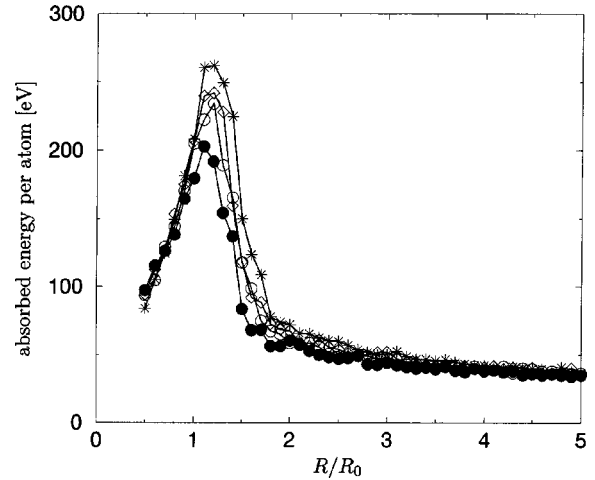


FIG. 7. Absorbed energy per atom as a function of the mean interionic distance for Ne_{16} (●), Ne_{20} (○), Ne_{25} (◇), and Ne_{30} (*).

If $4\pi r_s^3$ denotes the volume per atom, then $R = N^{1/3}r_s$ and

$$U(N+1) = U(N) + N^{2/3}Z^2/r_s. \quad (15)$$

With N as a continuous variable one is left with the differential equation

$$\frac{dU(N)}{dN} = \frac{N^{2/3}Z^2}{r_s}, \quad (16)$$

so that finally

$$U(N) = \frac{3}{5} \frac{N^{5/3}Z^2}{r_s}. \quad (17)$$

Hence, the potential energy per atom U/N increases with $N^{2/3}$ if the charge per atom is independent of N .

Proceeding from Ne to Ar clusters, one finds again that the effectivity of the ionization mechanism hardly changes on changing the cluster size, while the absorbed energy per atom increases with N , for the same reason as discussed above (we show here only the energy in Fig. 8). However, while the Ne clusters show only a little shift of R^* as a function of cluster size, the ratio of R^* to R_0 increases slightly more with increasing N for Ar. This is probably due to a larger down-shift of the atomic energy levels by the increased total amount of surrounding charge when N is increased. As can be seen from Fig. 5, a down-shift of the atomic energy levels leads to an increase in R^* . Since the electron release in argon clusters is larger than in Ne clusters, rendering this effect more pronounced for Ar clusters.

Since we have found a critical internuclear distance R^* with $R^* > R_0$ in all cases considered, it is not too surprising that we find a behavior analogous to the small clusters of Figs. 2 and 3 if the bigger clusters are allowed to expand freely. The results of these calculations, with the pulse normalization being identical to Sec. III, are shown in Figs. 9

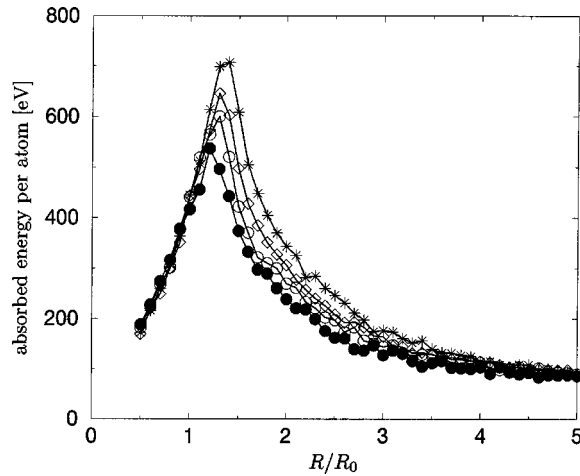


FIG. 8. Absorbed energy/atom as a function of the mean interionic distance for Ar_{16} (\bullet), Ar_{20} (\circ), Ar_{25} (\diamond), and Ar_{30} ($*$).

and 10. For clarity, we have plotted the total cluster charge instead of the average atomic charge, which is almost the same independent of N .

The overall structure of the curves is seen to be quite similar throughout the different cluster sizes. In the case of Ne clusters, the monotonic decrease that has been observed for Ne_{16} in Fig. 3 goes over into a small maximum with increasing N , which indicates that the enhanced ionization mechanism is slightly more efficient for larger clusters when the ions are allowed to move. One tendency that can be observed for the Ar clusters is that T^* increases with increasing N . We have seen in Fig. 8 that R^* increases also with N , so that the larger Ar clusters have to travel a longer distance until they reach a critical distance. For the Ne clusters, on the contrary, the curves show almost no shift in the T direction when N is changed. We will investigate the dependence of the expansion process on the various cluster parameters such as size and atom charge in closer detail in Sec. V.

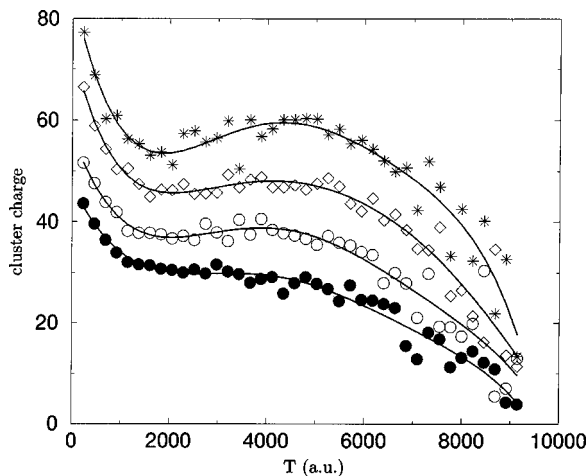


FIG. 9. Cluster charge as a function of pulse length for Ne_{16} (\bullet), Ne_{20} (\circ), Ne_{25} (\diamond), and Ne_{30} ($*$). Lines are to guide the eye.

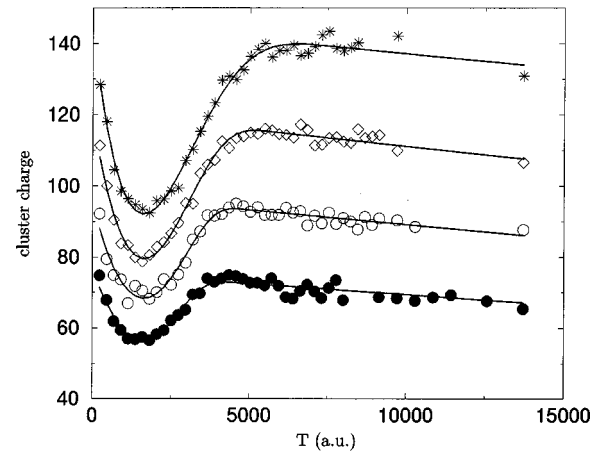


FIG. 10. Cluster charge as a function of pulse length for Ar_{16} (\bullet), Ar_{20} (\circ), Ar_{25} (\diamond), and Ar_{30} ($*$). Lines are to guide the eye.

B. The influence of the pulse normalization

Changing the laser intensity I in the case of H_2^+ , with just a single electron available, leads to a decrease of R^* when I is increased and vice versa [28]. For clusters, the situation is much more complicated because with increasing I lower lying energy levels will be ionized, so that it is *a priori* not clear in which way a change of the laser intensity (in a calculation with fixed nuclei) will influence the value of R^* . Figure 11 shows the static ionization yields for Ne_{16} and Xe_{16} under the influence of the pulse used so far (i.e., a peak intensity of $I_1 = 8.99 \times 10^{14} \text{ W/cm}^2$), compared to the result of a calculation with $I_2 = 2.19 \times 10^{15} \text{ W/cm}^2$ (in both cases the pulse was of the form (8) with $\omega = 0.055 \text{ a.u.}$ and $T = 55 \text{ fs}$). In all four cases R^* is larger than R_0 and can be reached by cluster expansion. The value of R^* is, if at all, only slightly decreased in the case of higher intensity: due to the large number of electrons involved the geometry of the problem is obviously not as sensitive to the laser field strength as in the H_2^+ case.

Of course, the ionization yield is higher when the intensity is increased. This leads to significantly shorter expansion times when the nuclei are allowed to move. Consequently, the optimal pulse lengths T^* are now shifted towards smaller values, as can be seen in Fig. 12 in accordance with our picture of the ionization process.

C. Enhanced ionization and circular polarization

So far all the results presented are expected to hold also for diatomic molecules. One main difference between such a molecule and a cluster is the molecular axis: the whole picture of ENIO as sketched in Fig. 5 relies on the fact that the polarization direction of the applied laser field coincides with the internuclear axis. And indeed, experiments as well as calculations with a polarization axis perpendicular to the molecular axis have shown no signature of enhanced ionization [26,29]. For the same reason ENIO is much less efficient under circular polarization.

On the other hand, a cluster is (in first approximation) spherically symmetric. Thus one would expect enhanced ion-

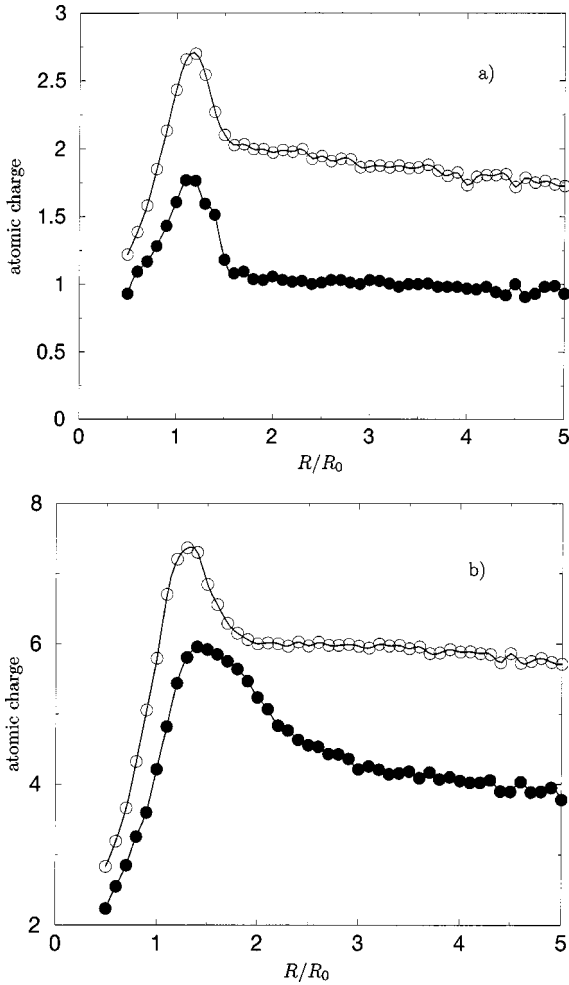


FIG. 11. Static ionization yield at the two intensities $I_1=8.99 \times 10^{14} \text{ W/cm}^2$ (●) and $I_2=2.19 \times 10^{15} \text{ W/cm}^2$ (○) for Ne_{16} (a) and Xe_{16} (b). Lines are to guide the eye.

ization to work also with circularly polarized light. To test this hypothesis, we have performed the same calculations as in the previous sections, but now with circularly polarized laser light. We have chosen the field strength of the laser such that the energy content of a pulse with a certain pulse length T remains constant when passing from linear to circular polarization. With this definition the maximum field strength is decreased by a factor of $\sqrt{2}$. As expected, ENIO also exists for circularly polarized laser pulses. Figure 13 shows the calculations with fixed nuclei; Fig. 14 shows the corresponding results with moving nuclei. In the case of static nuclei, we find that the ionization yield in the critical regime is almost as high for circular as for linear polarization (Fig. 4), in sharp contrast to the above-mentioned results for diatomic molecules. Consequently, when the nuclei are allowed to move, we also get qualitatively the same results (Fig. 14) as with linear polarization (Fig. 3). It is only for rather long pulses that in the case of Ne_{16} and Ar_{16} the ionization yield is significantly lower than in the linear case, which is due to the reduced maximum field strength. Summarizing our exploration of different parameters we find that ENIO for clusters is a rather robust phenomenon. This has

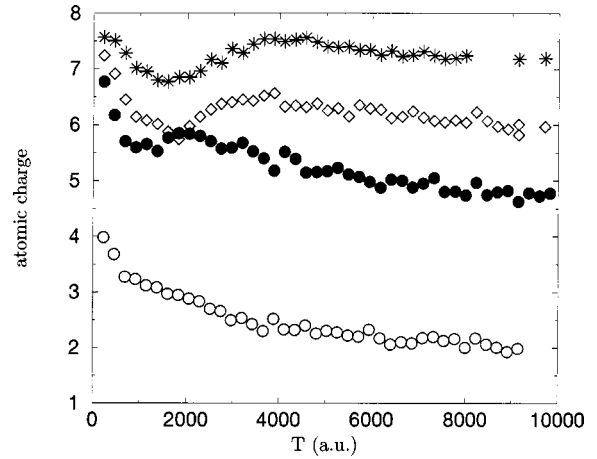


FIG. 12. Pulse length dependent ionization yields with a pulse energy corresponding to $I_2=2.19 \times 10^{15}$ and a pulse length of 20 cycles for Ne_{16} (○), Ar_{16} (●), Kr_{16} (◇), and Xe_{16} (*).

motivated us to ask if the optimum pulse length T^* can be quantitatively linked to the critical distance R^* .

V. ANALYTICAL FORMULA FOR THE COULOMB EXPLOSION

To isolate the relation of T^* to R^* we divide the time-dependent dynamics into three different phases (Fig. 15): phase I denotes the time from the onset of the laser pulse until 50% of the atoms in the cluster have lost one electron due to inner ionization. We will refer to this time as T_0 subsequently. Since some of the inner ionized electrons will leave the cluster, we can say that T_0 marks the beginning of the expansion process.

In this first phase inner ionization is dominated by atomic processes, the environment plays only a minor role. For a single atom (or ion) the time-dependent probability that the active electron is *not yet* ionized reads, in terms of the field-dependent and binding-energy-dependent ionization rate $w(f(t), E_b)$

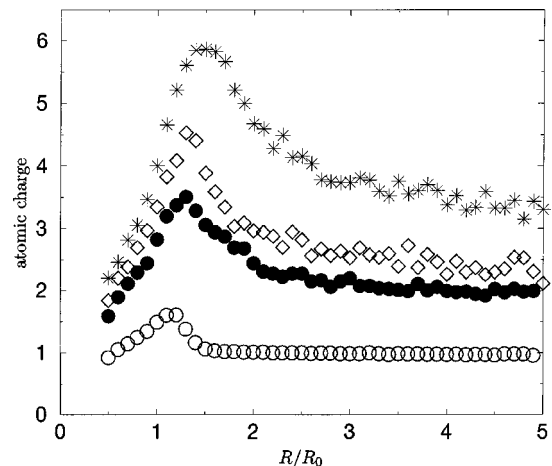


FIG. 13. Atomic charges with fixed nuclei and circular polarization for Ne_{16} (○), Ar_{16} (●), Kr_{16} (◇), and Xe_{16} (*). The pulse parameters are $F_0=0.16/\sqrt{2}$ a.u., $\omega=0.055$ a.u., and $T=55$ fs.

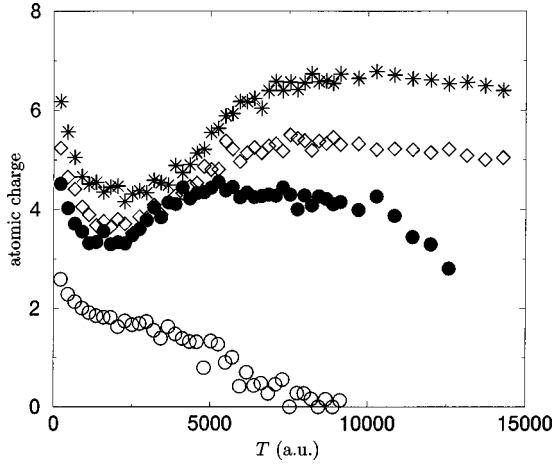


FIG. 14. Atomic charge for the same clusters as in Fig. 13 but as a function of pulse length T with moving nuclei.

$$P_{\text{neutral}}(t) = \exp\left(-\int_0^t w(f(t'), E_b) dt'\right), \quad (18)$$

where E_b denotes the binding energy. The probability that no electron has been ionized in a cluster consisting of N such atoms is given by

$$P_{\text{neutral}}^{\text{cluster}}(t) = [P_{\text{neutral}}(t)]^N. \quad (19)$$

The exponential dependence on N renders $P_{\text{neutral}}^{\text{cluster}}(t)$ practically a step function. Hence, the exact value (between 0 and 1) for the definition of T_0 is not relevant. We determine T_0 from $P_{\text{neutral}}^{\text{cluster}}(T_0) = 1/2$, which is tantamount to demanding that on average 50% of the atoms in the cluster are singly ionized at T_0 .

The second phase contains the cluster expansion up to the critical time T^* , when the critical cluster distance R^* is reached. Hence, the critical time is the sum of T_0 and the expansion time T_{exp} :

$$T^* = T_0 + T_{\text{exp}}. \quad (20)$$

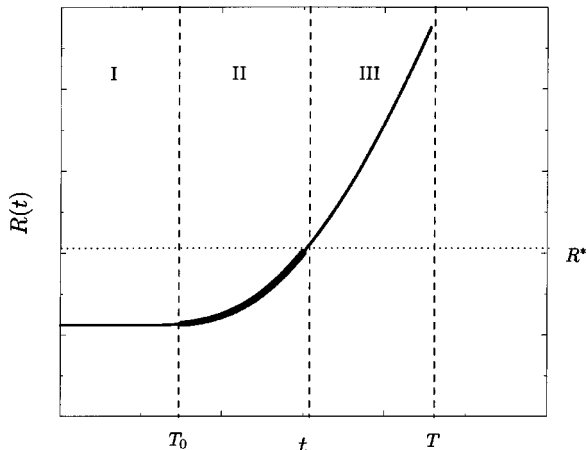


FIG. 15. Sketch of phases I, II, and III during the pulse (see text).

The third phase is finally the time from reaching R^* to the end of the pulse.

From T_0 until the end of the pulse, the total cluster charge increases from $Z = N/2$ to $Z = Z_{\text{final}}$. As a first approximation, we assume that the expansion from $R = R_0$ to $R = R^*$ is driven by an effective charge per atom $\bar{Z} = \alpha Z_{\text{final}}/N$ with a constant factor α that stands for the efficiency of the enhanced ionization mechanism. Furthermore, the expansion is assumed to be accomplished by the Coulomb repulsion of the nuclei only, i.e., we neglect the influence of the laser field as well as of the electronic dynamics on the expansion process. Under these two assumptions, we can use energy conservation to write

$$\sum_{i=1}^N \frac{M}{2} v_i^2 + \sum_{(i \neq j)=1}^N \frac{\bar{Z}^2}{r_{ij}(t)} = E, \quad (21)$$

where $r_{ij}(t) = |\vec{r}_i(t) - \vec{r}_j(t)|$, M is the atomic mass, and v_i is the respective atomic velocities. As a further approximation we assume that the expansion takes place in a homogenous and isotropic way, so that it can be described by a common expansion parameter $\lambda(t)$ with $\vec{r}_i(t) = \lambda(t)\vec{r}_i(0)$. Defining

$$K_0 := \sum_{i=1}^N \frac{1}{2} M r_i^2(0),$$

$$V_0 := \sum_{(i \neq j)=1}^N \frac{(Z_{\text{final}}/N)^2}{r_{ij}(0)}, \quad (22)$$

and taking into account that the kinetic energy is zero before the expansion, we may write the energy balance of Eq. (21) as

$$K_0 \lambda^2(t) + \frac{\alpha^2}{\lambda(t)} V_0 = \frac{\alpha^2}{\lambda(0)} V_0. \quad (23)$$

Finally, Eq. (23) may be rearranged as a differential equation for $\lambda(t)$,

$$\frac{d\lambda(t)}{dt} = \alpha \left[\left(1 - \frac{1}{\lambda(t)} \right) \frac{V_0}{K_0} \right]^{1/2}, \quad (24)$$

which can be solved analytically by separation of variables for the expansion time,

$$\begin{aligned} T_{\text{exp}} &= \sqrt{\frac{K_0}{V_0}} \frac{1}{\alpha} \left[\sqrt{\lambda(\lambda-1)} + \ln(\sqrt{\lambda-1} + \sqrt{\lambda}) \right] \\ &=: \sqrt{\frac{K_0 g(\lambda)}{V_0}} \frac{1}{\alpha}. \end{aligned} \quad (25)$$

The ratio K_0/V_0 determines the time scale for the expansion of the cluster. By replacing $r_{ij}(0)$, the distance between two ions in V_0 , with the average internuclear distance R according to Eq. (11) (which would be an exact approximation if all ions were placed on the surface of the cluster), we can estimate how this time scale depends on the characteristic variables of a cluster:

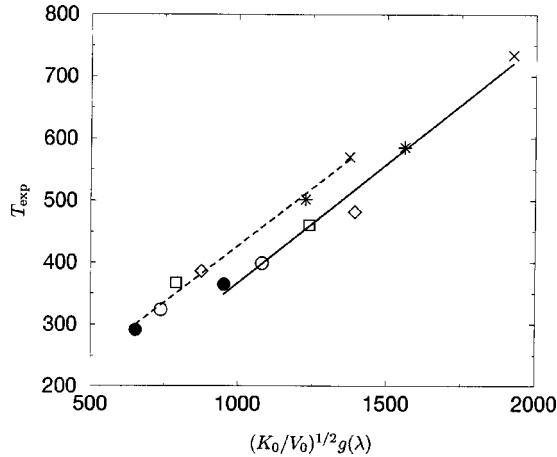


FIG. 16. Expansion time (numerical data) as a function of $(K_0/V_0)^{1/2}g(\lambda)$ and linear fits (see text). Two different energy normalizations were used: $F_0=0.16$ a.u. (solid line) and $F_0=0.25$ a.u. (dashed line), both at a frequency of $\omega=0.055$ a.u. and a pulse length of $T=55$ fs. Ar₁₆ (●), Ar₂₀ (○), Ar₂₅ (□), Ar₃₀ (◇), Kr₁₆ (*), and Xe₁₆ (×).

$$\frac{K_0}{V_0} \propto \frac{MR^3}{(N-1)(Z_{\text{final}}/N)^2}. \quad (26)$$

From this equation we can read off how the expansion process changes when the number of atoms, N , is changed while keeping all other parameters fixed: if $V_{\text{atom}}=4/3\pi r_s^3$ is the volume of one atom inside the cluster, then $R^3=Nr_s^3$. Hence, the time scale of the expansion is governed by the factor $N/(N-1)$, which depends only weakly on N .

Scaling of the optimal pulse length

Using Eq. (25) we are able to set up a relation between the optimal pulse lengths for various clusters if we make one last assumption: the factor α , which determines the ratio between the average atomic charge \bar{Z} driving the expansion up to R^* and the final charge per atom after the pulse Z_{final}/N , is identical for all clusters. If this hypothesis was true, then $1-\alpha$ would be a universal measure for the efficiency of the ENIO mechanism.

If α is the same for all clusters, we get from Eq. (25) a linear relation between the expansion time T_{exp} and $g(\lambda)(T_0/V_0)^{1/2}$, different for each cluster. This prediction is confirmed by Fig. 16 that shows the expansion times $T_{\text{exp}}=T^*/2-T_0$ as a function of the cluster-dependent values of $(K_0/V_0)^{1/2}g(\lambda)$ for different clusters. We have obtained λ from the respective static calculations for each cluster. A lin-

ear fit to the data yields $\alpha=0.38$ and $\alpha=0.37$ for energy normalized pulses at $F_0=0.16$ and $F_0=0.25$, respectively. The correlation coefficient is in both cases higher than 0.99. Hence, α is the same for different clusters, and it is even almost the same for different energy normalizations of the laser pulse. This result *a posteriori* justifies the approximations we have made in establishing our expansion model.

The fact that α remains almost the same on changing the pulse normalization is certainly an unexpected result; it is probably valid only for a limited range of pulse energy contents, if one thinks of α as a measure for the efficiency of ENIO. At least in the limit of a very large pulse energy, when the electric field of the laser is larger than the electric field from the charges in the cluster, we expect the ENIO mechanism to play no important role any more, since the cluster geometry will be washed out. However, the good agreement of the linear fit in Fig. 16 with our numerical data for each of the two normalizations separately points to a deeper scaling relation between the various clusters, the reason for which will be explored in future work.

VI. SUMMARY AND CONCLUSION

We have developed a quasiclassical model for a small rare-gas cluster in strong laser fields. This model allows us to investigate not only the influence of several parameters, such as the atomic element and the cluster size, but also the characteristics of the applied laser field. We have shown that, as a function of pulse length, the energy absorption as well as the ionization yield of all but the Ne clusters show a clear maximum when the energy content of the pulse is kept fixed. This behavior has been attributed to the existence of a critical average internuclear distance R^* , whose origin could be explained by generalizing the CREI or ENIO concept from diatomic molecules to small rare-gas clusters. It was shown that this mechanism is stable against a change of system parameters, even when switching from linear to circular polarization. This is a pronounced difference between clusters and molecules.

Finally, we were able to condense the absorption and expansion process into a simple model and obtained an analytical expression connecting the expansion time and the cluster properties. The validity of this expression has been confirmed by our numerical data.

ACKNOWLEDGMENTS

We would like to thank Ulf Saalman for helpful discussions and the DFG for financial support within the Gerhard Hess program.

- [1] F. Calvayrac, E. Suraud, and P. Reinhard, J. Phys. B **31**, 1367 (1998).
 [2] F. Calvayrac, P. Reinhard, E. Suraud, and C. Ullrich, Phys. Rep. **337**, 493 (2000).
 [3] W. Tappe, R. Flesch, E. Rühl, R. Hoekstra, and T. Schlathöler,

- Phys. Rev. Lett. **88**, 143401 (2002).
 [4] L. Köller, M. Schumacher, J. Köhn, S. Teuber, J. Tiggesbäumker, and K. Meiwes-Broer, Phys. Rev. Lett. **82**, 3783 (1999).
 [5] T. Ditmire, T. Donnelly, A. Rubenchik, R. Falocone, and M.

- Perry, Phys. Rev. A **53**, 3379 (1996).
- [6] J. Zweiback, T. Ditmire, and M. Perry, Phys. Rev. A **59**, R3166 (1999).
- [7] M. Lezius, S. Dobosz, D. Normand, and M. Schmidt, Phys. Rev. Lett. **80**, 261 (1998).
- [8] J. Purnell, E. Snyder, S. Wei, and A.W. Castleman, Chem. Phys. Lett. **229**, 333 (1994).
- [9] E. Springate, N. Hay, J. Tisch, M. Mason, T. Ditmire, M. Hutchinson, and J. Marangos, Phys. Rev. A **61**, 063201 (2000).
- [10] T. Ditmire, J. Zweiback, V. Yanovsky, T. Cowan, G. Hays, and K. Wharton, Nature (London) **398**, 489 (1999).
- [11] C. Siedschlag and J.M. Rost, Phys. Rev. Lett. **89**, 173401 (2002).
- [12] T. Zuo and A. Bandrauk, Phys. Rev. A **52**, R2511 (1995).
- [13] T. Seideman, M. Yvanov, and P. Corkum, Phys. Rev. Lett. **75**, 2819 (1995).
- [14] V. Veniard, R. Taieb, and A. Maquet, Phys. Rev. A **65**, 013202 (2002).
- [15] I. Last and J. Jortner, Phys. Rev. A **60**, 2215 (1999).
- [16] I. Last and J. Jortner, Phys. Rev. A **62**, 013201 (2000).
- [17] M. Ammosov, N. Delone, and V. Krainov, Sov. Phys. JETP **64**, 1191 (1986).
- [18] D. Bauer and P. Mulser, Phys. Rev. A **59**, 569 (1999).
- [19] K. Ishikawa and T. Blenski, Phys. Rev. A **62**, 063204 (2000).
- [20] P. Channell and C. Scovel, Nonlinearity **3**, 231 (1990).
- [21] C. Rose-Petruck, K. Schafer, K. Wilson, and C. Barthy, Phys. Rev. A **55**, 1182 (1997).
- [22] T. Ditmire, Phys. Rev. A **57**, R4094 (1998).
- [23] L.D. Landau and E.M. Lifshitz, *Quantenmechanik* (Akademie-Verlag, Berlin, 1960).
- [24] W. Ekardt, Phys. Rev. Lett. **52**, 1925 (1984).
- [25] J. Posthumus, L. Frasiniski, A. Giles, and K. Codling, J. Phys. B **28**, L349 (1995).
- [26] A. Bandrauk and J. Ruel, Phys. Rev. A **59**, 2153 (1999).
- [27] I. Kawata, H. Kono, and A. Bandrauk, Phys. Rev. A **64**, 043411 (2001).
- [28] J. Posthumus, A. Giles, M. Thompson, W. Shaikh, A. Langley, L. Frasiniski, and K. Codling, J. Phys. B **29**, L525 (1996).
- [29] S. Banerjee, G.R. Kumar, and D. Mathur, Phys. Rev. A **60**, R25 (1999).
- [30] See <http://brain.ch.cam.ac.uk/jon/structures/LJ/> for a compilation of potential minima.